Small-Signal Stability Support from Dynamically Configurable Grid-Forming/Following Inverters for Distribution Systems

Preprint

Lizhi Ding,[1] Yuhua Du,[1] Xiaonan Lu,[1] Shuan Dong,[2] Andy Hoke,[2] and Jin Tan[2]

1 Temple University
2 National Renewable Energy Laboratory

Presented at the IEEE Energy Conversion Congress and Exposition
Detroit, Michigan
October 9-13, 2022

NREL is a national laboratory of the U.S. Department of Energy
Office of Energy Efficiency & Renewable Energy
Operated by the Alliance for Sustainable Energy, LLC

This report is available at no cost from the National Renewable Energy Laboratory (NREL) at www.nrel.gov/publications.

Contract No. DE-AC36-08GO28308

Conference Paper
NREL/CP-6A40-83340
November 2022

Small-Signal Stability Support from Dynamically Configurable Grid-Forming/Following Inverters for Distribution Systems

Preprint

Lizhi Ding,[1] Yuhua Du,[1] Xiaonan Lu,[1] Shuan Dong,[2] Andy Hoke,[2] and Jin Tan[2]

1 Temple University
2 National Renewable Energy Laboratory

Suggested Citation
Ding, Lizhi, Yuhua Du, Xiaonan Lu, Shuan Dong, Andy Hoke, and Jin Tan. 2022. *Small-Signal Stability Support from Dynamically Configurable Grid-Forming/Following Inverters for Distribution Systems: Preprint*. Golden, CO: National Renewable Energy Laboratory. NREL/CP-6A40-83340. https://www.nrel.gov/docs/fy23osti/83340.pdf.

NREL is a national laboratory of the U.S. Department of Energy
Office of Energy Efficiency & Renewable Energy
Operated by the Alliance for Sustainable Energy, LLC

This report is available at no cost from the National Renewable Energy Laboratory (NREL) at www.nrel.gov/publications.

Contract No. DE-AC36-08GO28308

Conference Paper
NREL/CP-6A40-83340
November 2022

National Renewable Energy Laboratory
15013 Denver West Parkway
Golden, CO 80401
303-275-3000 • www.nrel.gov

NOTICE

This work was authored in part by the National Renewable Energy Laboratory, operated by Alliance for Sustainable Energy, LLC, for the U.S. Department of Energy (DOE) under Contract No. DE-AC36-08GO28308. Funding provided by the U.S. Department of Energy Office of Energy Efficiency and Renewable Energy Solar Energy Technologies Office Award Number 37772. The views expressed herein do not necessarily represent the views of the DOE or the U.S. Government. The U.S. Government retains and the publisher, by accepting the article for publication, acknowledges that the U.S. Government retains a nonexclusive, paid-up, irrevocable, worldwide license to publish or reproduce the published form of this work, or allow others to do so, for U.S. Government purposes.

Cover Photos by Dennis Schroeder: (clockwise, left to right) NREL 51934, NREL 45897, NREL 42160, NREL 45891, NREL 48097, NREL 46526.

Small-Signal Stability Support From Dynamically Configurable Grid-Forming/Following Inverters for Distribution Systems

Lizhi Ding
College of Engineering
Temple University
Philadelphia, USA
lizhi.ding@temple.edu

Yuhua Du
College of Engineering
Temple University
Philadelphia, USA
yuhua.du@temple.edu

Xiaonan Lu
College of Engineering
Temple University
Philadelphia, USA
xiaonan.lu@temple.edu

Shuan Dong
Grid Planning and Analysis Center
National Renewable Energy Laboratory
Golden, USA
shuan.dong@nrel.gov

Andy Hoke
Power Systems Engineering Center
National Renewable Energy Laboratory
Golden, USA
andy.hoke@nrel.gov

Jin Tan
Grid Planning and Analysis Center
National Renewable Energy Laboratory
Golden, USA
jin.tan@nrel.gov

***Abstract*—The growth of inverter-based resources (IBRs) in modern power systems can challenge system stability since they do not natively provide inertia, prompting a need to develop new methods to address the potential instabilities. In this paper, a dynamically configurable grid-forming (GFM) and grid-following (GFL) control is proposed, which enables inverters to flexibly transition to support system needs. The operation mode transition between GFM and GFL controls is adopted as an additional degree of control flexibility to adjust the small-signal stability margin. In addition, a holistic and detailed small-signal model for a distribution feeder that captures the dynamics from both synchronous generators (SGs) and IBRs is also derived and used to evaluate the effectiveness of the proposed GFM/GFL controls to augment the system small-signal stability margin. Case studies with varying levels of IBRs were implemented in MATLAB/Simulink to demonstrate the effectiveness of the proposed approach.**

***Index Terms*—grid-following control, grid-forming control, operation mode transition, small-signal stability analysis**

I. Introduction

With the increase of inverter-based resources (IBRs) (e.g., wind and solar energy), the modern power grid is gradually dominated by static power electronic inverters rather than synchronous generators (SGs) [1]; however, the replacement of SGs with inverters reduces the grid inertia and changes the fundamental dynamic characteristics of bulk power systems, which makes the entire system susceptible to instabilities under disturbances and poses additional operational challenges [2].

Pulse-width modulation inverters are often used as the interface to connect the IBRs and the power grid. The existing grid-interactive inverters are generally in grid-following (GFL) control mode [3]; however, GFL inverters cannot actively establish grid frequency and voltage, and they could trigger stability issues when the level of IBRs is high. In contrast, grid-forming (GFM) inverters can actively establish frequency and voltage at the local inverter level, which makes them widely used in microgrids and large-scale distribution systems [4]; however, the interactions and couplings among GFM inverters and SGs might introduce undesired oscillatory modes [5].

To further improve system stability with large amounts of IBRs, numerous studies have been conducted in the literature. A virtual inertia emulator-based model predictive control is used in [6] to address the challenge of frequency regulation introduced by a larger number of inverters. To address the stability issue brought by the high shares of IBRs, a linear quadratic regulator-based optimization technique is used in [7] for the inverters with virtual synchronous machine control to adjust the emulated inertia based on the system frequency disturbance. To solve the problem of less effective voltage regulation due to the low X/R ratios in the distribution system, a voltage margin control is used in [8] to coordinate the photovoltaic inverter and battery energy storage system for voltage regulation without any communication.

Due to the low inertia, grid-interactive inverters could become less robust in the face of various disturbances than SGs. The usual way to ensure a sufficient stability margin is to fine-tune the parameters of the designed controllers [9]; however, the conventional control parameter tuning could reach a bottleneck considering the limited number of adjustable control parameters. Because IBRs naturally feature a high control bandwidth, it is possible to enable additional control functions for flexible-mode transitions at each IBR [10]; therefore, the operation modes could be leveraged as an additional control variable to maximize the small-signal stability margin of the

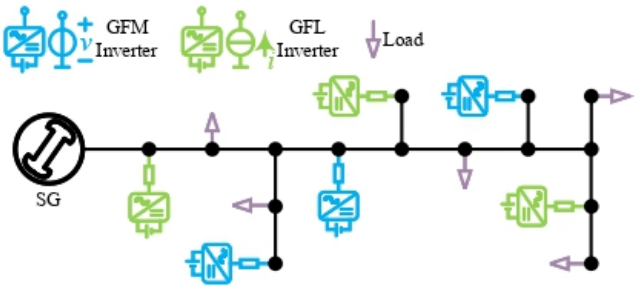

Fig. 1. A typical distribution feeder with inverters with either GFM or GFL controls.

entire system and improve the overall dynamic performance.

The rest of this work is organized as follows: In Section II, the mathematical modeling of a distribution system considering the impacts of SGs and IBRs is obtained. The holistic small-signal model of a distribution system with SGs and inverters is developed in Section III. In Section IV, case studies aiming at system small-signal stability enhancement are discussed, with emphasis on the amount of energy provided by IBRs. Section V summarizes the work and draws the conclusion.

II. Mathematical Modeling of the Distribution Feeder

As shown in Fig. 1, a typical distribution feeder with IBRs comprises inverters with either GFM or GFL controls. The upstream system is represented by an aggregated SG. To analyze the small-signal stability of the entire system, a mathematical model of the distribution system is derived first. The system can be divided into four subsections: inverters, SG, load, and network. The mathematical modeling of each part will be obtained separately and then used to derive the holistic small-signal model of the entire system.

A. Modeling Inverters with GFM Control

A muti-loop diagram is developed for the inverters with GFM control, including droop control, voltage control, and current control. The inverter configuration is shown in Fig. 2 (a), and the droop control shown in Fig. 2 (b) is implemented to establish the inverter frequency and voltage [11]. Thus:

$$\begin{cases} \omega_{inv} = \omega_n - m_p(P_{inv} - P_0) \\ V_{inv} = V_n - n_q(Q_{inv} - Q_0) \end{cases} \tag{1}$$

where ω_{inv} and V_{inv} are the inverter frequency and output voltage, respectively; ω_n and V_n are the nominal frequency and voltage, respectively; m_p and n_q are the droop gains; P_{inv} and Q_{inv} are the inverter output active and reactive power, respectively; and P_0 and Q_0 are the power set points.

The low-pass filters (LPFs) with the cutoff frequency of ω_c are used for the active and reactive power measurements. Combined with the differential equation of the phase angle,

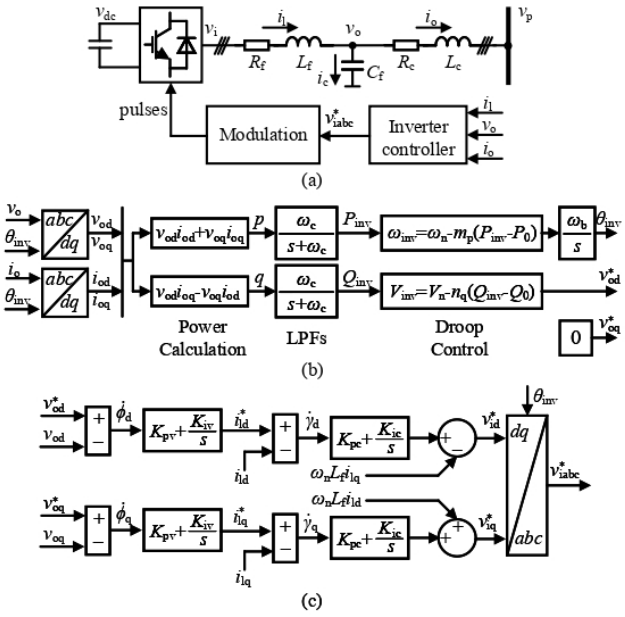

Fig. 2. GFM inverters configuration and control diagram: (a) inverter configuration, (b) GFM inverter droop control. (c) GFM inverter inner loops.

the differential equations related to the power controller are obtained as [12]:

$$\begin{cases} \dot{\theta}_{inv} = \omega_b \omega_{inv} \\ \dot{P}_{inv} = -\omega_c P_{inv} + \omega_c(v_{od} i_{od} + v_{oq} i_{oq}) \\ \dot{Q}_{inv} = -\omega_c Q_{inv} + \omega_c(v_{od} i_{oq} - v_{oq} i_{od}) \end{cases} \tag{2}$$

where ω_b is the base value of the angular frequency; ω_c is the cutoff frequency of the LPFs; v_{od} and v_{oq} are the inverter output voltage in the $d-$ and $q-$ axis, respectively; and i_{od} and i_{oq} are the inverter output current in the $d-$ and $q-$ axis, respectively. Note that all variables are expressed in the per-unit system unless otherwise noted.

Further, as shown in Fig. 2 (c), the proportional-integral (PI) controllers are deployed for the voltage and current loops to enhance the controllability. The intermediate variables ϕ_d and ϕ_q are defined for simplifying the equations of the PI controllers in the voltage loop; the intermediate variables γ_d and γ_q are defined for simplifying the equations of the PI controllers in the current loop; they are defined as:

$$\begin{cases} \dot{\phi}_d = v^*_{od} - v_{od}, \quad \dot{\phi}_q = v^*_{oq} - v_{oq} \\ \dot{\gamma}_d = i^*_{ld} - i_{ld}, \quad \dot{\gamma}_q = i^*_{lq} - i_{lq} \end{cases} \tag{3}$$

along with:

$$\begin{cases} v^*_{od} = V_{inv}, \quad v^*_{oq} = 0 \\ i^*_{ld} = K_{pv}(v^*_{od} - v_{od}) + K_{iv}\phi_d \\ i^*_{lq} = K_{pv}(v^*_{oq} - v_{oq}) + K_{iv}\phi_q \end{cases} \tag{4}$$

where v^*_{od} and v^*_{oq} are the inverter output voltage references in the $d-$ and $q-$ axis, respectively; i^*_{ld} and i^*_{lq} are the inverter-side inductor current references in the $d-$ and $q-$

axis, respectively; and K_{pv} and K_{iv} are the PI gains in the voltage loop.

The LCL filter is interfaced with the inverter and the point of common coupling (PCC) to mitigate the switching harmonics. The differential equations that are used to describe the dynamics of the LCL filter are given as [12]:

$$\begin{cases} \dot{i}_{ld} = \omega_b(\dfrac{v_{id} - v_{od}}{L_f} - \dfrac{R_f}{L_f} i_{ld} + \omega_{inv} i_{lq}) \\ \dot{i}_{lq} = \omega_b(\dfrac{v_{iq} - v_{oq}}{L_f} - \dfrac{R_f}{L_f} i_{lq} - \omega_{inv} i_{ld}) \\ \dot{v}_{od} = \omega_b(\dfrac{i_{ld} - i_{od}}{C_f} + \omega_{inv} v_{oq}) \\ \dot{v}_{oq} = \omega_b(\dfrac{i_{lq} - i_{oq}}{C_f} - \omega_{inv} v_{od}) \\ \dot{i}_{od} = \omega_b(\dfrac{v_{od} - v_{pd}}{L_c} - \dfrac{R_c}{L_c} i_{od} + \omega_{inv} i_{oq}) \\ \dot{i}_{oq} = \omega_b(\dfrac{v_{oq} - v_{pq}}{L_c} - \dfrac{R_c}{L_c} i_{oq} - \omega_{inv} i_{od}) \end{cases} \tag{5}$$

where v_{id} and v_{iq} are the inverter terminal voltage in the $d-$ and $q-$ axis, respectively; i_{ld} and i_{lq} are the inverter-side inductor current in the $d-$ and $q-$ axis, respectively; R_f and L_f are the resistance and inductance of the inverter-side inductor, respectively; C_f in the capacitance of the filter capacitor; R_c and L_c are the resistance and inductance of the PCC-side inductor, respectively; and v_{pd} and v_{pq} are the PCC voltage in the $d-$ and $q-$ axis, respectively. Note that the assumption is adopted that the inverter terminal voltage outputs the demanded voltage [13]; thus:

$$\begin{cases} v_{id} = v_{id}^* = K_{pc}(i_{ld}^* - i_{ld}) + K_{ic}\gamma_d - \omega_n L_f i_{lq} \\ v_{iq} = v_{iq}^* = K_{pc}(i_{lq}^* - i_{lq}) + K_{ic}\gamma_q + \omega_n L_f i_{ld} \end{cases} \tag{6}$$

where v_{id}^* and v_{iq}^* are the inverter terminal voltage references in the $d-$ and $q-$ axis, respectively; and K_{pc} and K_{ic} are the PI gains in the current loop.

To coordinate with other generation units, loads, and the network, the inverter output current and the PCC voltage should be converted between the individual reference frame and the common reference frame with the following transformation [13]:

$$\begin{cases} i_{oD} = i_{od}\cos(\theta_{inv}) - i_{oq}\sin(\theta_{inv}) \\ i_{oQ} = i_{od}\sin(\theta_{inv}) + i_{oq}\cos(\theta_{inv}) \\ v_{pd} = v_{pD}\cos(\theta_{inv}) + V_{pQ}\sin(\theta_{inv}) \\ v_{pq} = -v_{pD}\sin(\theta_{inv}) + V_{pQ}\cos(\theta_{inv}) \end{cases} \tag{7}$$

where i_{oD} and i_{oQ} are the inverter output current in the common $D-$ and $Q-$ axis, respectively; and v_{pD} and v_{pQ} are the PCC voltage in the common $D-$ and $Q-$ axis, respectively.

B. Modeling Inverters with GFL Control

A muti-loop diagram is also developed for inverters with GFL control, as shown in Fig. 3; however, the outer power loop is configured to track the power references rather than to implement the droop control like the GFM inverters. Besides, the capacitor-current-feedback active damping method is used to address the resonance issue given that the LCL filter is used in the interface inverter [14]. Additionally, the angular frequency of the inverter with GFL control can be obtained through a phase-locked loop (PLL) [15]. The dynamic modeling of the current loop, LCL filter, and the coordinate transformation is similar to the counterparts of GFM inverters and will not be detailed here for simplification.

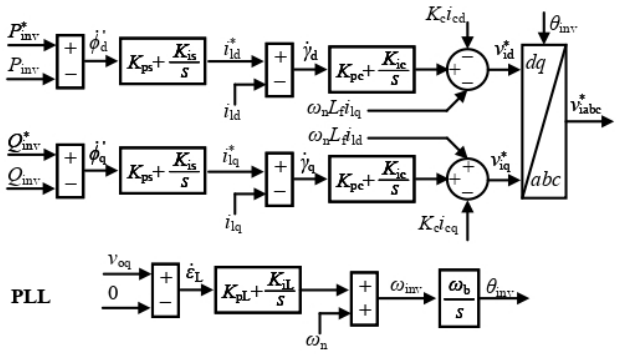

Fig. 3. Control diagram of GFL inverters.

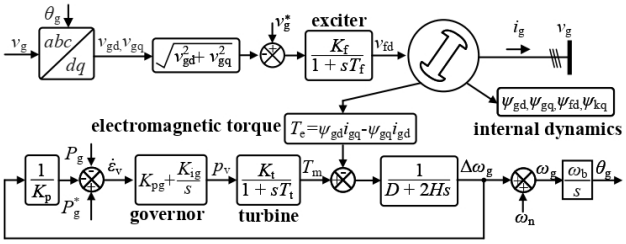

Fig. 4. Block diagram of SGs.

For the PLL, the block diagram is shown in Fig. 3, and the intermediate variable ε_L is defined for the PI controller; thus:

$$\begin{cases} \dot{\varepsilon}_L = v_{oq} - 0 \\ \dot{\theta}_{inv} = \omega_b(K_{pL} v_{oq} + K_{iL}\varepsilon_L + \omega_n) \end{cases} \tag{8}$$

where K_{pL} and K_{iL} are the PI gains in the PLL.

For the power loop, the intermediate variables $\phi_d^{'}$ and $\phi_q^{'}$ are defined for the PI controllers:

$$\dot{\phi}_d^{'} = P_{inv}^* - P_{inv}, \quad \dot{\phi}_q^{'} = Q_{inv}^* - Q_{inv} \tag{9}$$

along with:

$$\begin{cases} i_{ld}^* = K_{ps}(P_{inv}^* - P_{inv}) + K_{is}\phi_d^{'} \\ i_{lq}^* = K_{ps}(Q_{inv}^* - Q_{inv}) + K_{is}\phi_q^{'} \end{cases} \tag{10}$$

where P_{inv}^* and Q_{inv}^* are the active and reactive power references for the GFL inverter, respectively; and K_{ps} and K_{is} are the PI gains in the power loop.

C. Modeling SGs, Loads, and Lines

A salient pole SG is studied, and the control diagram is shown in Fig. 4. The dynamics of the stator, exciter, and

q-axis amortisseur circuit are considered, and the models of the exciter and turbine are simplified to the first-order representations [16]:

$$G_f(s) = \frac{K_f}{1+sT_f}, \quad G_t(s) = \frac{K_t}{1+sT_t} \tag{11}$$

where $G_f(s)$ and $G_t(s)$ are the transfer functions of the exciter and turbine, respectively; K_f and T_f are the first-order model gain and time constant of the exciter, respectively; and K_t and T_t are the first-order model gain and time constant of the turbine, respectively.

A PI-based governor is used to regulate the output power of the turbine [17]. An intermediate variable ε_v is used for the PI controller; thus:

$$\begin{cases} \varepsilon_v = P_g^* + \dfrac{\omega_n - \omega_g}{K_p} - P_g \\ p_v = K_{pg}(P_g^* + \dfrac{\omega_n - \omega_g}{K_p} - P_g) + K_{ig}\varepsilon_v \end{cases} \tag{12}$$

where p_v is the valve position used as the input variable for the turbine; ω_g is the SG operating frequency; P_g^* and P_g are the SG active power set point and output, respectively; K_{pg} and K_{ig} are the PI control gains for the governor; and K_p is the droop gain of the SG.

Further, the voltage equations and flux linkage equations are used to describe the internal electrical dynamics. They are [16]:

$$2H\frac{d\omega_g}{dt} = T_m - T_e - D(\omega_g - \omega_n) \tag{13}$$

$$\begin{cases} v_{gd} = -R_s i_{gd} - \omega_g \psi_{gq} + \dfrac{d\psi_{gd}}{\omega_b dt} \\ v_{gq} = -R_s i_{gq} + \omega_g \psi_{gd} + \dfrac{d\psi_{gq}}{\omega_b dt} \\ v_{fd} = R_{fd} i_{fd} + \dfrac{d\psi_{fd}}{\omega_b dt} \\ v_{kq} = R_{kq} i_{kq} + \dfrac{d\psi_{kq}}{\omega_b dt} \end{cases} \tag{14}$$

$$\begin{cases} \psi_{gd} = -L_d i_{gd} + L_{ad} i_{fd}, \psi_{gq} = -L_q i_{gq} + L_{aq} i_{kq} \\ \psi_{fd} = L_{fd} i_{fd} - L_{ad} i_{gd}, \psi_{kq} = L_{kq} i_{kq} - L_{aq} i_{gq} \end{cases} \tag{15}$$

where T_m is the SG mechanical torque; T_e is the SG electromagnetic torque and $T_e = \psi_{gd} i_{gq} - \psi_{gq} i_{gd} \approx v_{gd} i_{gd} + v_{gq} i_{gq}$; H is the SG inertia constant; D is the damping factor; $\psi_{gd}(L_d), \psi_{gq}(L_q), \psi_{fd}(L_{fd})$, and $\psi_{kq}(L_{kq})$ are the flux linkages (self-inductances) in the stator d-axis, stator q-axis, exciter, and q-axis amortisseur circuit; $v_{gd}(i_{gd}), v_{gq}(i_{gq}), v_{fd}(i_{fd})$, and $v_{kq}(i_{kq})$ are the voltages (currents) in the stator d-axis, stator q-axis, exciter, and q-axis amortisseur circuit; R_s, R_{fd}, and R_{kq} are the resistance in the stator, exciter, and q-axis amortisseur circuit; and L_{ad} and L_{aq} are the mutual inductance.

In this work, the constant impedance model is implemented for all loads and lines [12]; hence, the mathematical modeling of the loads and lines are similar to those shown in (5) and will not be detailed here for simplification.

III. Small-Signal Stability Analysis of the Distribution Feeder

A. Holistic Small-Signal Modeling of the Full Feeder

After considering the dynamics from the mutiple control loops and LCL filter, the small-signal representation of the ith inverter with GFM or GFL control is summarized as:

$$\Delta\dot{\mathbf{X}}_{v,i} = \mathbf{A}_{v,i}\Delta\mathbf{X}_{v,i} + \mathbf{B}_{v,i}\Delta\mathbf{V}_{pDQ,i} + \mathbf{B}_{v\omega,i}\Delta\omega_{com} \tag{16a}$$

$$\Delta\mathbf{I}_{oDQ,i} = \mathbf{C}_{v,i}\Delta\mathbf{X}_{v,i} \tag{16b}$$

where $\mathbf{X}_{v,i} = [\delta_{inv,i}, P_{inv,i}, Q_{inv,i}, \phi_{d,i}, \phi_{q,i}, \gamma_{d,i}, \gamma_{q,i}, i_{ld,i}, i_{lq,i}, v_{od,i}, v_{oq,i}, i_{od,i}, i_{oq,i}]^T$ for the GFM inverter, and $\delta_{inv,i}$ is the phase angle of the ith inverter with respect to the common reference frame with the angular frequency ω_{com}; $\mathbf{X}_{v,i} = [\varepsilon_{L,i}, \delta_{inv,i}, P_{inv,i}, Q_{inv,i}, \phi^{'}_{d,i}, \phi^{'}_{q,i}, \gamma_{d,i}, \gamma_{q,i}, i_{ld,i}, i_{lq,i}, v_{od,i}, v_{oq,i}, i_{od,i}, i_{oq,i}]^T$ for the GFL inverter; and $v_{pDQ,i} = [v_{pD,i}, v_{pQ,i}]^T$; $i_{oDQ,i} = [i_{oD,i}, i_{oQ,i}]^T$;

Similarly, the complete small-signal model of the SG can be summarized as:

$$\Delta\dot{\mathbf{X}}_g = \mathbf{A}_g\Delta\mathbf{X}_g + \mathbf{B}_g\Delta\mathbf{V}_{gDQ} + \mathbf{B}_{g\omega}\Delta\omega_{com} \tag{17a}$$

$$\Delta\mathbf{I}_{gDQ} = \mathbf{C}_g\Delta\mathbf{X}_g, \Delta\omega_g = \mathbf{C}_{g\omega}\Delta\mathbf{X}_g \tag{17b}$$

where $\mathbf{X}_g = [\delta_g, \omega_g, \psi_{gd}, \psi_{gq}, \psi_{fd}, \psi_{kq}, \varepsilon_v, T_m, v_{fd}]^T$; δ_g is the phase angle of the SG with respect to the common reference frame; $\mathbf{V}_{gDQ} = [v_{gD}, v_{gQ}]^T$; and $\mathbf{I}_{gDQ} = [i_{gD}, i_{gQ}]^T$.

Both the loads and lines are modeled in the common D-Q frame, whose small-signal representations are adopted from the existing work [13]. By combing the small-signal models of all the subsystems, including SG, inverters, loads, and the network, the holistic small-signal model of the distribution system under study is summarized as:

$$\Delta\dot{\mathbf{X}}_{sys} = \mathbf{A}_{sys}\Delta\mathbf{X}_{sys} \tag{18}$$

where $\mathbf{X}_{sys} = [\mathbf{X}_g, \mathbf{X}_{inv}, \mathbf{X}_d, \mathbf{X}_l]^T$; $\mathbf{X}_{inv} = [\mathbf{X}_{v,1}, \cdots, \mathbf{X}_{v,N}]^T$, where N is the number of the inverters; $\mathbf{X}_d$ is the state vector of all loads; and $\mathbf{X}_l$ is the state vector of all lines. Note that the operating points can be obtained by using the method proposed in our previous work [18].

B. Small-Signal Stability Quantification

The eigenvalues of the system matrix $\mathbf{A}_{sys}$ in (18) are denoted as λ_i for $i = 1, \cdots, M$. A zero eigenvalue would be found in λ_i due to the invariant common reference frame. This zero eigenvalue is denoted as λ_1 and excluded in the subsequent analysis. The system small-signal stability margin is defined as the maximum real part of the nonzero eigenvalues [19]:

$$\Omega_m = max[Re(\lambda_2), \cdots, Re(\lambda_M)] \tag{19}$$

If $\Omega_m < 0$, the system is locally asymptotically stable. Additionally, a smaller Ω_m indicates a larger small-signal stability margin. Considering the various disturbances or fluctuations of the real power system in both the short-term and long-term timescales, Ω_m needs to be sufficiently negative to ensure stable system operation.

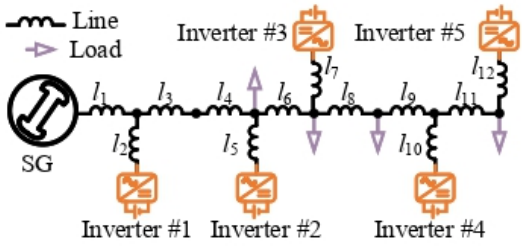

Fig. 5. Test system.

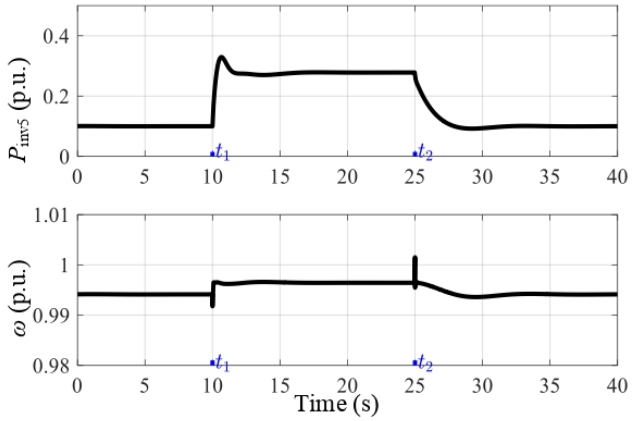

Fig. 6. Test results for dynamically configurable operation of inverters.

IV. Case Study

A. Test System

To verify the principle of the operation mode transition, a test system with one SG, 5 inverters, 5 loads, and 12 lines is studied, and the system configuration is schematically shown in Fig. 5. The SG is operated by following the control diagram as shown in Fig. 4. The inverters are operated by either GFM or GFL controls, and the lines and loads are represented by the constant impedance models. The system parameters, including the main power circuit and the control diagram of all the components, are listed in Table I.

B. Dynamically Configurable Operation of Inverters

The dynamically configurable operation of inverters between the GFM and GFL controls can be realized by freezing the integral values in the inner loops at the time when the operation mode transition occurs. The frozen values will be used as the initial ones when the new operation mode starts. To demonstrate the proposed method, a test case is designed in MATLAB/Simulink. The operation mode of Inverter #5 is designed to be changed from GFL to GFM control at time t_1 and then back to GFL control at time t_2. The output active power and load frequency of Inverter #5 are obtained to show the dynamic responses. As shown in Fig. 6, the operation mode transition can be realized through the proposed method without large overshoots.

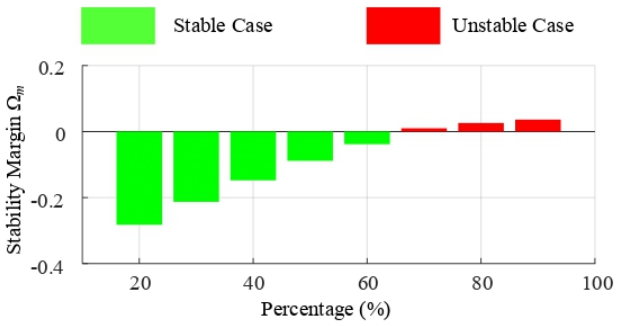

Fig. 7. Stability margin variations with fixed inverter operation modes.

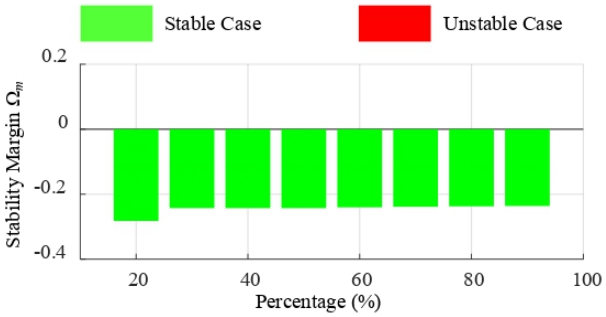

Fig. 8. Stability margin variations with flexible inverter operation modes.

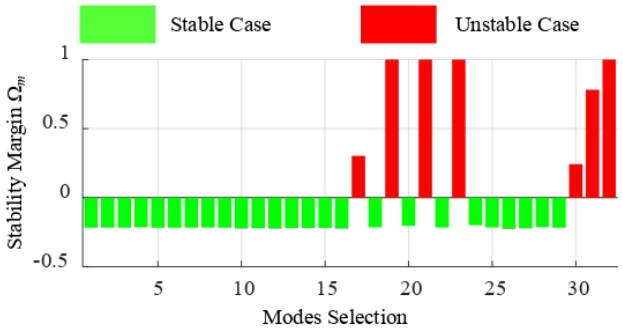

Fig. 9. Stability margin when the output power of the five inverters are 0.1, 0.1, 0.1, 0.5, and 0.1 p.u., respectively.

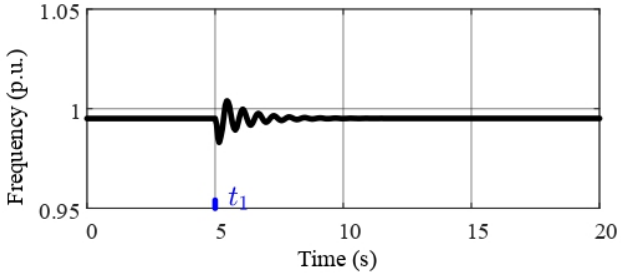

Fig. 10. System frequency variation under 90% IBR percentage for the stable case.

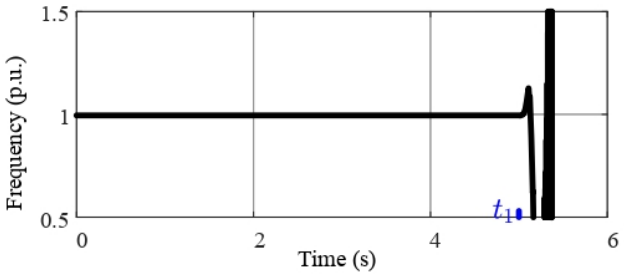

Fig. 11. System frequency variation under 90% IBR percentage for the unstable case.

TABLE I
SYSTEM PARAMETERS

Parameters	Values
SG Parameters	$H = 2.6$ s, $D = 1$ p.u., $K_{pg} = 10$, $K_{ig} = 4$, $K_t = 0.8$, $T_t = 0.5$, $K_f = 1.2$, $T_f = 0.2$, $R_s = 0.002$ p.u., $L_d = 1.08$ p.u., $L_q = 1.05$ p.u., $L_{ad} = 0.99$ p.u., $L_{aq} = 0.96$ p.u., $R_{fd} = 0.0004$ p.u., $L_{fd} = 1.08$ p.u., $R_{kq} = 0.0037$ p.u., $L_{kq} = 1.39$ p.u.
Inverter Parameters	$R_f = 0.02$ p.u., $L_f = 0.10$ p.u., $C_f = 0.10$ p.u., $R_c = 0.02$ p.u., $L_c = 0.05$ p.u., $m_p = 0.02$, $n_q = 0.02$, $K_{pv} = 0.5$, $K_{iv} = 2.8$, $K_{pc} = 1.0$, $K_{ic} = 2.0$, $K_c = 0.1$, $\omega_c = 10\pi$ rad/s
Network Parameters ($\times 10^{-3}$ p.u.)	$R_{l1} = 14.6$, $L_{l1} = 27.2$, $R_{l2} = 4.6$, $L_{l2} = 8.5$ $R_{l3} = 9.1$, $L_{l3} = 17.0$, $R_{l4} = 10.2$, $L_{l4} = 102.5$ $R_{l5} = 87.6$, $L_{l5} = 163.2$, $R_{l6} = 7.3$, $L_{l6} = 13.6$ $R_{l7} = 6.7$, $L_{l7} = 10.3$, $R_{l8} = 9.1$, $L_{l8} = 17.0$ $R_{l9} = 9.1$, $L_{l9} = 17.0$, $R_{l10} = 3.4$, $L_{l10} = 5.2$ $R_{l11} = 67.5$, $L_{l11} = 103.5$, $R_{l12} = 8.1$, $L_{l12} = 12.4$
Load Parameters (p.u.)	$R_{load} = 4.8075$, $L_{load} = 0.9620$

*Base values are selected as: $S_b = 100$ MVA, and $\omega_b = 120\pi$ rad/s; all the inverters and loads adopt the same parameters.

C. System Stability Augmentation with Varying IBR Percentages

The effectiveness of the dynamically configurable operation of inverters with either GFM or GFL controls on small-signal stability enhancement is validated by conducting case studies with varying IBR percentages. As the IBR percentage moves toward 100%, the derived system small-signal stability margin is shown in Fig. 7, where all the inverters are operated in GFL mode. Note that the inertia of the SG is proportionally reduced as the IBR percentage increases because the increase of the IBRs is usually accompanied by the displacement of SGs and the consequent reduction in the system inertia [20]. As the IBR percentage increases, the system is gradually destabilized. As designed, the operation mode of each inverter could be flexibly adjusted, and the updated system stability margins are shown in Fig. 8. By actively implementing the desired operation mode transition, the system small-signal stability can be maintained even with a high IBR percentage, which could not be done when the operation modes are fixed. Additionally, to highlight the impacts of the operation modes, when the IBR percentage is 90%, the system small-signal stability margin under different operation mode combinations is presented in Fig. 9, which shows that it is possible to secure stable system operation by implementing the properly selected inverter operation mode.

The system stability margin is also validated in the time domain. When the five inverters are operated in GFM, GFL, GFL, GFL, and GFM modes, respectively (i.e., the $15th$ bar in Fig. 9), a disturbance is introduced to the output power of Inverter #4 at t_1, and the corresponding system frequency variations are presented in Fig. 10. The system remains stable after the disturbance, which agrees with the stability analysis in Fig. 9; however, when the inverters are operated in GFL, GFM, GFM, GFL, and GFM modes (i.e., the $19th$ bar in Fig. 9), respectively, with the same power set points, the system cannot maintain stable operation under the same disturbance, as shown in Fig. 11, which also agrees with the stability analysis in Fig. 9.

V. CONCLUSION

A detailed mathematical model of a distribution feeder with dynamics from both SGs and IBRs is derived and then used to obtain the holistic small-signal model of the distribution system. The effectiveness of the operation mode transition of the grid-interactive inverters is demonstrated by the case studies with varying percentages of IBRs. Results show that the IBR percentage could be further increased, even to 100%, by leveraging the operation mode as an additional control variable with the enhanced system small-signal stability.

ACKNOWLEDGMENTS

This work was authored in part by the National Renewable Energy Laboratory, operated by Alliance for Sustainable Energy, LLC, for the U.S. Department of Energy (DOE) under Contract No. DE-AC36-08GO28308. Funding provided by the U.S. Department of Energy Office of Energy Efficiency and Renewable Energy Solar Energy Technologies Office Award Number 37772. The U.S. Government retains and the publisher, by accepting the article for publication, acknowledges that the U.S. Government retains a nonexclusive, paid-up, irrevocable, worldwide license to publish or reproduce the published form of this work, or allow others to do so, for U.S. Government purposes. The views expressed herein do not necessarily represent the views of the U.S. Department of Energy or the United States Government.

REFERENCES

[1] Q. Peng, Q. Jiang, Y. Yang, T. Liu, H. Wang, and F. Blaabjerg, "On the stability of power electronics-dominated systems: Challenges and potential solutions," *IEEE Transactions on Industry Applications*, vol. 55, no. 6, pp. 7657–7670, 2019.

[2] U. Markovic, O. Stanojev, P. Aristidou, E. Vrettos, D. Callaway, and G. Hug, "Understanding small-signal stability of low-inertia systems," *IEEE Transactions on Power Systems*, vol. 36, no. 5, pp. 3997–4017, 2021.

[3] R. Rosso, X. Wang, M. Liserre, X. Lu, and S. Engelken, "Grid-forming converters: Control approaches, grid-synchronization, and future trends—a review," *IEEE Open Journal of Industry Applications*, vol. 2, pp. 93–109, 2021.

[4] Y. Du, X. Lu, H. Tu, J. Wang, and S. Lukic, "Dynamic microgrids with self-organized grid-forming inverters in unbalanced distribution feeders," *IEEE Journal of Emerging and Selected Topics in Power Electronics*, vol. 8, no. 2, pp. 1097–1107, 2020.

[5] L. Ding, X. Lu, and J. Tan, "Comparative small-signal stability analysis of grid-forming and grid-following inverters in low-inertia power systems," in *IECON 2021 – 47th Annual Conference of the IEEE Industrial Electronics Society*, 2021, pp. 1–6.

[6] N. Sockeel, J. Gafford, B. Papari, and M. Mazzola, "Virtual inertia emulator-based model predictive control for grid frequency regulation considering high penetration of inverter-based energy storage system," *IEEE Transactions on Sustainable Energy*, vol. 11, no. 4, pp. 2932–2939, 2020.

[7] U. Markovic, Z. Chu, P. Aristidou, and G. Hug, "Lqr-based adaptive virtual synchronous machine for power systems with high inverter penetration," *IEEE Transactions on Sustainable Energy*, vol. 10, no. 3, pp. 1501–1512, 2019.

[8] L. Wang, F. Bai, R. Yan, and T. K. Saha, "Real-time coordinated voltage control of pv inverters and energy storage for weak networks with high pv penetration," *IEEE Transactions on Power Systems*, vol. 33, no. 3, pp. 3383–3395, 2018.

[9] S. Harasis, K. Mahmoud, S. Albatran, K. Alzaareer, and Q. Salem, "Dynamic performance evaluation of inverter feeding a weak grid considering variable system parameters," *IEEE Access*, vol. 9, pp. 126 104–126 116, 2021.

[10] X. Li, H. Zhang, M. B. Shadmand, and R. S. Balog, "Model predictive control of a voltage-source inverter with seamless transition between islanded and grid-connected operations," *IEEE Transactions on Industrial Electronics*, vol. 64, no. 10, pp. 7906–7918, 2017.

[11] K. De Brabandere, B. Bolsens, J. Van den Keybus, A. Woyte, J. Driesen, and R. Belmans, "A voltage and frequency droop control method for parallel inverters," *IEEE Transactions on Power Electronics*, vol. 22, no. 4, pp. 1107–1115, 2007.

[12] A. Aderibole, H. H. Zeineldin, and M. Al Hosani, "A critical assessment of oscillatory modes in multi-microgrids comprising of synchronous and inverter-based distributed generation," *IEEE Transactions on Smart Grid*, vol. 10, no. 3, pp. 3320–3330, 2019.

[13] N. Pogaku, M. Prodanovic, and T. C. Green, "Modeling, analysis and testing of autonomous operation of an inverter-based microgrid," *IEEE Transactions on Power Electronics*, vol. 22, no. 2, pp. 613–625, 2007.

[14] D. Pan, X. Ruan, C. Bao, W. Li, and X. Wang, "Capacitor-current-feedback active damping with reduced computation delay for improving robustness of lcl-type grid-connected inverter," *IEEE Transactions on Power Electronics*, vol. 29, no. 7, pp. 3414–3427, 2014.

[15] S. Golestan, J. M. Guerrero, and J. C. Vasquez, "Three-phase plls: A review of recent advances," *IEEE Transactions on Power Electronics*, vol. 32, no. 3, pp. 1894–1907, 2017.

[16] P. Kundur, *Power system stability and control*. New York, NY, USA: McGraw-Hill, 1994.

[17] M. Eremia and M. Shahidehpour, *Handbook of electrical power system dynamics: modeling, stability, and control*. Hoboken, NJ, USA: John Wiley & Sons, 2013.

[18] L. Ding, Y. Men, Y. Du, X. Lu, B. Chen, J. Tan, and Y. Lin, "Region-based stability analysis of resilient distribution systems with hybrid grid-forming and grid-following inverters," in *2020 IEEE Energy Conversion Congress and Exposition (ECCE)*, 2020, pp. 3733–3740.

[19] F. Molnar, T. Nishikawa, and A. E. Motter, "Asymmetry underlies stability in power grids," *Nature communications*, vol. 12, no. 1, pp. 1–9, 2021.

[20] D. Pattabiraman, J. Tan, V. Gevorgian, A. Hoke, C. Antonio, and D. Arakawa, "Impact of frequency-watt control on the dynamics of a high DER penetration power system," in *2018 IEEE Power Energy Society General Meeting (PESGM)*, 2018, pp. 1–5.